We are IntechOpen, the world's leading publisher of Open Access books Built by scientists, for scientists

4,800
Open access books available

122,000
International authors and editors

135M
Downloads

Our authors are among the

154
Countries delivered to

TOP 1%
most cited scientists

12.2%
Contributors from top 500 universities

WEB OF SCIENCE™

Selection of our books indexed in the Book Citation Index in Web of Science™ Core Collection (BKCI)

Interested in publishing with us?
Contact book.department@intechopen.com

Numbers displayed above are based on latest data collected.
For more information visit www.intechopen.com

18

Laser Diode Gas Spectroscopy

Pablo Pineda Vadillo
University of Dublin, Trinity College Dublin
Ireland

1. Introduction

The use of laser sources for optical spectroscopy experimentation is a well-established, cross-disciplinary field with an enormous number of applications in research areas as broad as Physics, Chemistry or Biology (Demtröder, 1996). The high optical intensity achieved with these types of sources, along with the extraordinary monochromaticity of their optical output, has a huge impact in spectroscopy research. In particular, the application to gas sensing in weak absorption spectral regions significantly benefits from the specific properties of laser. Gas species exhibit well-defined, complex spectral absorption structures that require the utilisation of tuneable, high resolution and spectrally narrow sources to be resolved. Such requirements are fulfilled by several types of Tuneable Diode Lasers (TDL's) readily available from the optical telecommunication industry, where much work was done during the last decades to develop and improve the characteristics of these laser devices. Further technology development and intensive research has lead to TDL's of high optical power and narrow emission linewidth to be routinely available for research groups across the world, thus opening the possibility for investigation of gas absorption processes of increasing complexity and very narrow spectral scales. In addition, advances in manufacturing technology have enabled the design and fabrication of new photonic microstructures in parallel to the development of laser sources. The combination of both factors has thus multiplied the possibilities for challenging gas-sensing research, which in turn reveals new fundamental characteristics of gaseous systems whose study requires more and more stable, narrow linewidth and powerful laser sources.

This chapter contains a summary of the main properties and operational principles of laser diodes in connection to gas spectroscopy. Analysis is presented related to the main laws and principles applying to light absorption by gases, though many concepts can be extended to other types of absorbing media. Description of the main detection techniques is included along with selected experimental results to complement the theoretical discussions. Finally, a selection of references gives the reader the option to get a deeper insight into this rich and multidisciplinary research area.

2. Light absorption and gas spectra

2.1 Light absorption by a medium

Light of angular frequency $w=2\pi v$ travelling through a material of refractive index n can experience a number of different processes. In general, part of the incoming radiation is

absorbed by the medium, while the rest is free to propagate until it eventually escapes, retaining its original propagation direction –transmitted light- or presenting some deviation - scattered light-. *Absorption* processes are accompanied by *dispersion* of the light, the latter defined by the change in phase velocity of light from its value in vacuum *c*. These properties of the interaction of electromagnetic radiation with an absorbing medium are classically described by an oscillator model for the atomic electrons, leading to the definition of a complex refractive index to explain both effects.

The basic rules governing linear absorption of light by a medium of refractive index *n* are summarized in the so-called Beer-Lambert law. Consider a light beam travelling along the *Z* direction of an absorbing medium of number density *C* and transverse area *A*. The total number of illuminated molecules for a material thickness *dz* is *CAdz*, though the effective area presented by this ensemble is given by $\sigma CAdz$, σ being the cross-section for absorption/scattering in this case. Thus, the total probability for a molecule of being either absorbed or scattered out of the beam will be (Garrett, 2006)

$$\frac{dI_Z}{I_Z} = \frac{\sigma CAdz}{A} \tag{1}$$

which upon integration gives the so-called Beer-Lambert law for linear attenuation

$$I = I_0 e^{-\sigma Cz} = I_0 e^{-\mu z} \tag{2}$$

If scattering is neglected, then the *linear attenuation coefficient* $\mu=\sigma C$ is equal to the *linear absorption coefficient* α and the Beer-Lambert relation can be rewritten in the form

$$I(\lambda) = I_0(\lambda) e^{-\alpha(\lambda)z} \tag{3}$$

where the dependence of the absorption coefficient on the wavelength λ of the incoming light is explicitly indicated. In Optical Spectroscopy, the Beer-Lambert law is usually expressed in terms of the incoming plane wave angular frequency $\omega = 2\pi c/\lambda = 2\pi\upsilon$, and the medium, frequency-dependent, complex refractive index $n(\omega)$. The treatment presented by Measures (Measures, 1988 - special emphasis on the use of tuneable laser diodes in laser absorption measurements) is followed here, hence it can be written

$$n(\omega) = \eta(\omega) + \frac{1}{2} i x(\omega) \tag{4}$$

where the real part of the refractive index $\eta(\omega)$ accounts for the dispersion of the light as it travels through the medium and the imaginary term $\chi(\omega)$ is related to its absorption properties. The oscillator model for an electromagnetic wave travelling through a medium of complex refractive index (4) leads to the well-known *Kramers-Kronig* dispersion relations relating these two terms, which apply in the proximity of an atomic transition frequency ω_0 and for the case of the imaginary term reads (Measures, 1988)

$$x(\omega) = \frac{Ne^2 f_0 \gamma}{4 \in_0 m_e \omega \left[(\omega - \omega_0)^2 + (\gamma / 2)^2 \right]} \tag{5}$$

where N is the number density of oscillators, e and m_e the charge and mass of the electron, respectively, and γ the damping constant for the oscillator model. The absorption coefficient introduced in (3) is related to the imaginary term of the refractive index so that

$$\alpha(\omega) = \frac{\omega x(\omega)}{c} \tag{6}$$

where c is the speed of light in vacuum. It is thus convenient to refer to the frequency-dependent form for the Beer-Lambert law for consistency,

$$I(\omega) = I_0(\omega)e^{-\alpha(\omega)z} \tag{7}$$

2.2 Gas molecular structures and absorbing transitions

In this chapter absorption will be studied regarding gas species. Optical absorption by a gas occurs when the energy carried by an incoming photon is resonant with the difference between two molecular energy states. The distribution of energy states for a gas is determined by three types of motion, namely *rotational* (molecules rotating about its centre of mass, CM), *vibrational* (vibrations of individual/sets of atoms within a molecule with a static CM) and *electronic* (electrons moving within the molecule). Depending on the particular symmetry of the targeted molecule, the energy levels are distributed in a specific manner. In addition, these three types of motion interact with each other according to established selection/combination rules, giving rise to very complex absorption spectra in some cases.

In section 5 of this chapter some experimental results are presented regarding acetylene gas (C_2H_2), targeting absorbing transitions which belong to the *rotational-vibrational combination band* $\upsilon_1+\upsilon_3$. The main properties of such bands can be described as follows. First of all, we are working within a *vibrational* band characterized by its corresponding vibration frequency υ. Secondly, the band is not centred at a *fundamental* vibration frequency υ_i, but at a *combination* value $\upsilon_i + \upsilon_j$ (υ_1 and υ_3 correspond to two of the total five normal vibration modes available for acetylene (Steinfeld, 2005)). Thirdly, the absorbing transitions occur between *rotational* energy levels whose distribution is embedded on top of the vibrational modes. This type of rotational-vibrational energy map is illustrated in figure 1, corresponding to some of the relevant energy levels and transitions in the simple case of a diatomic molecule (this figure is adapted from the very comprehensive book on molecular spectroscopy by Banwell (Banwell & McCash, 1994)). Note how the absorption spectrum schematically shown at the foot of the figure consists of several absorption lines with varying intensities, due to the fact that not all rotational J levels are populated to the same degree in thermal equilibrium. The $\upsilon_1+\upsilon_3$ band for acetylene is centred at a wavelength of approximately 1525.8 nm within the Near Infra Red (NIR) region, where the intensity of absorption lines is much smaller than in the IR fundamental absorption region. This is a very important fact to take into account, because these weak transitions are difficult to detect unless very sensitive detection schemes are implemented or the gas concentration is high. A more extended, good comprehensive summary of main molecular concepts relevant to spectroscopy can be found in Weldon (Weldon, 2005), while an

extremely detailed treatment on Infrared and Raman spectra of polyatomic molecules was published by Herzberg and can be consulted for advanced topics (Herzberg, 1945).

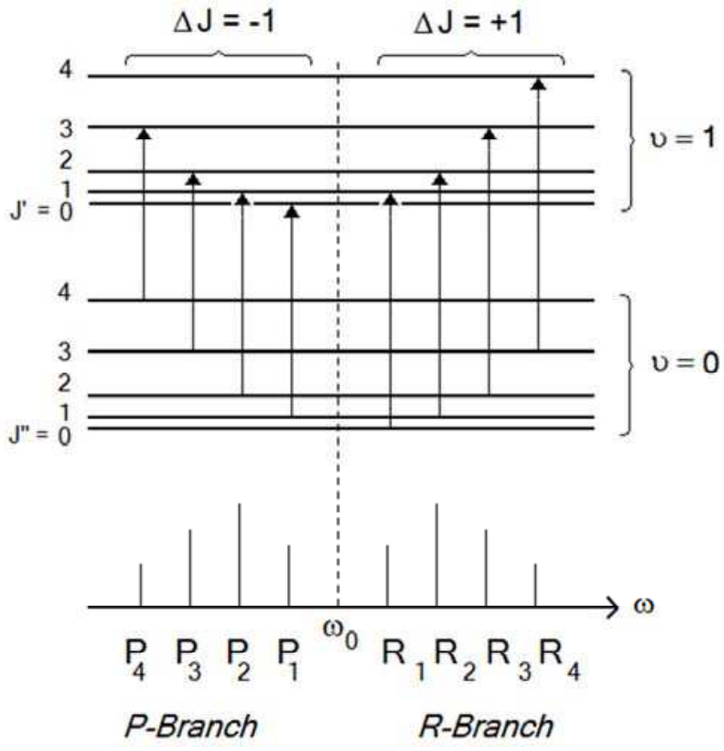

Fig. 1. Schematic diagram for the rotational (J) – vibrational (υ) energy level distribution of a diatomic molecule (figure adapted from (Banwell & McCash, 1994)).

2.3 Broadening processes and absorption lineshapes

In spectroscopic applications, the Beer-Lambert law (7) can be written as

$$I(\tilde{\upsilon},z) = I_0 e^{-\kappa(\tilde{\upsilon})z_D} = I_0 e^{-\kappa(\tilde{\upsilon})Cz} \tag{8}$$

where $\kappa(\tilde{\upsilon})$ is the absorption coefficient at the frequency $\tilde{\upsilon}$ when the latter is expressed in inverse length units according to the relations

$$\tilde{\upsilon}\left(cm^{-1}\right) \equiv \frac{1}{\lambda(cm)} \equiv \frac{\upsilon(Hz)}{c\left(cm\ s^{-1}\right)} = \frac{\omega(Hz)}{2\pi c\left(cm\ s^{-1}\right)} \tag{9}$$

and $z_D = Cz$ is the so-called *optical density* with generic units of concentration times length (using the notation introduced in equation 2). The absorption $\kappa(\tilde{\upsilon})$ thus has units of reciprocal concentration times length, and is normally expressed in $1/(\text{molecules cm}^{-3}\,\text{cm})$ or $(\text{cm}^2/\text{molecule})$. We will simplify the notation from now on and use υ when referring to $\tilde{\upsilon}(cm^{-1})$ for more clarity. Because the shape of the absorption profile is generally of interest, the absorption coefficient can be rewritten in a more useful form according to

$$\kappa(\upsilon) = Sg(\upsilon - \upsilon_0) \tag{10}$$

where the so-called *linestrength* S is essentially the integrated absorption coefficient and includes information about the absorption profile shape,

$$S = \int_{-\infty}^{\infty} \kappa(\upsilon) d\upsilon \tag{11}$$

while the *lineshape function* $g(\upsilon - \upsilon_o)$ is normalised according to

$$g(\upsilon - \upsilon_0) = C\phi(\upsilon - \upsilon_0), \quad \int_{-\infty}^{\infty} g(\upsilon - \upsilon_0) d\upsilon = 1 \tag{12}$$

and allows intensity profiles described by $\phi(\upsilon-\upsilon_o)$ to be compared directly. A common choice is that the concentration C in (8) is expressed in molecules/cm^3 since these units are independent of temperature (if the absorbing medium is a gas and concentration is expressed in terms of pressure units, then its equation of state needs to be specified). In that case S has units of cm/molecule and the lineshape function $g(\upsilon-\upsilon_0)$ is given in cm according to (10).

Real absorption profiles for gaseous systems are not δ-like functions but exhibit some finite linewidth due to several broadening effects. The convolution of these effects determines the final lineshape function for the absorbing transition, empirically characterized by its Full Width at Half Maximum (FWHM) as illustrated in figure 2. Several physical processes affect the absorption profiles during typical experimental work, and can be classified/described according to different criteria.

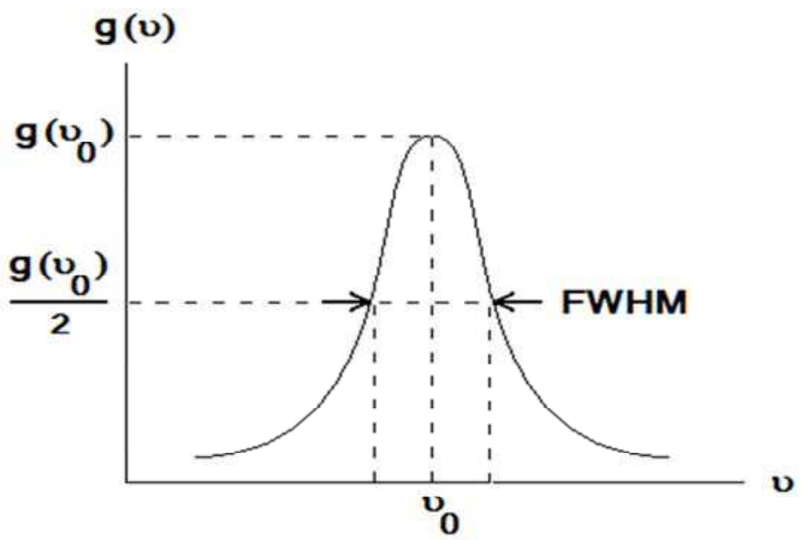

Fig. 2. Lineshape function g(υ-υo) characterized by its Full Width at Half Maximum (FWHM).

Three main broadening mechanisms contribute to the experimental measurements presented at the end of the chapter. The most straightforward mechanism is that related to the well-known **Doppler** effect, where a molecule with a non-zero velocity component in

the propagation direction of the radiation field absorbs a photon at some frequency shifted from the resonant transition frequency *at rest*. The distribution of molecular speeds across the whole ensemble of active molecules is given by the Maxwell-Boltzmann distribution, which tells us which molecules fall in which velocity class. The final result is a spectral absorption profile given, to a first approximation commonly used, by a **Gaussian** lineshape function of the form (Measures, 1988)

$$g_D(\upsilon-\upsilon_0)=\left(\frac{2}{\Delta\upsilon_D}\right)\sqrt{ln2/\pi}\exp\left[-\frac{2(\upsilon-\upsilon_0)^2 ln2}{\Delta\upsilon_D}\right] \tag{13}$$

with a FWHM of

$$\Delta\upsilon_D=\frac{2\upsilon_0}{c}\sqrt{2kTln2/m} \tag{14}$$

Note how the magnitude of the Doppler broadening increases with temperature as $T^{1/2}$ and resonant frequency υ_0. During the experimental results presented in section 5 both the gas temperature and the operating frequency (within some small tuning range) are kept constant, and so the associated Doppler width is essentially constant.

The second effect to take into account is the spectral broadening introduced by molecular **collision** processes. Several models exist to explain such an effect, but we will restrict the discussion to the simple Lorentz model followed in (Measures, 1988). This model assumes that the electron oscillation described by the classical absorption model halts on collision and then restarts with a completely random phase, totally unrelated to that prior to the collision event. This incoherence eventually leads to molecular absorption at a frequency different than the resonant value, and it can be demonstrated that the collisionally broadened lineshape function is given by a **Lorentzian** curve

$$g_L(\upsilon-\upsilon_0)=\left(\frac{\Delta\upsilon_L}{2\pi}\right)\frac{1}{\left[(\upsilon-\upsilon_0)^2+\Delta\upsilon_L^2/4\right]} \tag{15}$$

A rather cumbersome expression for the FWHM ($\Delta\upsilon_L$) of this normalised lineshape is found in the treatment by Measures that we are following, so for explanation purposes we can refer to Svelto (Svelto, 1998) where the FWHM for a collisionally-broadened transition is given in a different approach by

$$\Delta\upsilon_L=\frac{1}{\pi\tau_C}=\Delta\upsilon_L^0\left(\frac{P}{P_0}\right)\left(\frac{T_0}{T}\right)^{1/2} \tag{16}$$

where τ_C represents the mean time between collisions and the pressure and temperature dependences for the linewidth parameter have been taken from (Measures, 1988) again ($\Delta\upsilon^0_L$ is the linewidth at standard pressure and temperature conditions). The most important fact illustrated by relation (16) for experimental purposes is that, at a fixed gas temperature, the collisional broadening increases linearly with pressure. Note that this type of broadening can be introduced not only by intermolecular collisions, but also by collisions of the active

molecules with the **walls** of the gas hosting structure. The latter effect is small when gas cells of the order of tens of centimetres of height/widths are used, but in the specific case of the Hollow-Core PBF used in section 5 the wall collisions play a crucial role (the diameter of the utilised fibre was approximately $d \approx 11\ \mu m$). However this fibre-related broadening is in practice almost indistinguishable from the transit-time effect explained next, with treatment in the literature using one of the two possible approaches.

The last of the three significant broadening mechanisms to take into account during experiments in PBF fibres is that related to the **transit-time** effect: under certain physical conditions the transit time of gas molecules *moving* across the laser beam becomes smaller than their excited state lifetime. This *effective* shorter lifetime eventually gives rise to a spread of the absorbing frequencies around the resonant value, as time and optical frequency can be related via the Heisenberg uncertainty relations. It can be demonstrated (Demtröder, 1996) that the spectral intensity profile for atoms perpendicularly traversing a Gaussian laser beam of 1/e diameter $2w$ with a velocity v is given by a **Gaussian** curve

$$I(\omega) = I_0 \exp\left[-(\omega - \omega_0)^2 \frac{w^2}{2v^2} \right] \tag{17}$$

with a transit-time limited FWHM

$$\Delta\upsilon_{TT} \approx 0.4v / w \tag{18}$$

Figure 3 further illustrates the previous discussion. Note that this effect depends on the geometry of the fibre, but also on the *gas temperature*: the value for the mean velocity of the gas molecules is given by the kinetic theory of gases and ultimately depends on the temperature T for a fixed molecular mass M (Nave, 2009).

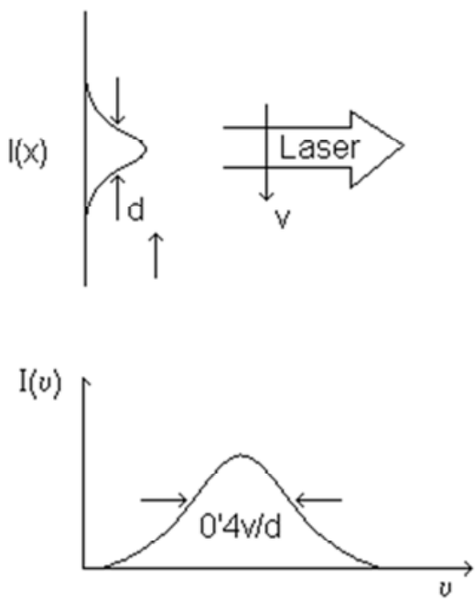

Fig. 3. Transit-time broadening of an absorbing transition (figure adapted from (Demtröder, 1996)).

Thus, the main broadening processes affecting an absorbing transition during the experimental work presented at the end of the chapter have been both qualitatively and mathematically described. Note that, in a real situation, the final absorption profile is the result of more than one broadening factor at the same time and cannot be described by the *pure* lineshapes described above. In such case the so-called *Voigt* profile must be used, a convolution of a Lorentzian and Gaussian profiles that must be evaluated numerically (Measures, 1988). A graphical comparison between the normalised Lorentzian, Gaussian and Voigt profiles with the same area under the curve $A = 1$ is included in figure 4, where it can be observed that the Voigt profile essentially follows a Lorentzian profile near its wings and a Gaussian curve around the line centre. Further analysis of absorption lineshapes in gases can be found in (Lepère, 2004; Varghese & Hanson, 1984).

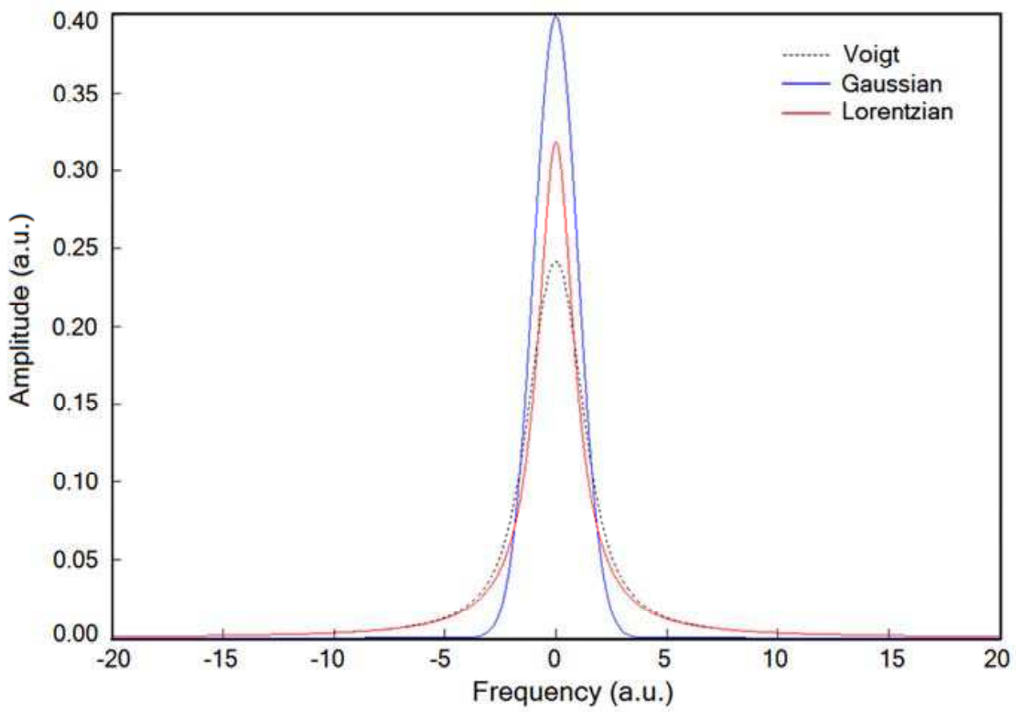

Fig. 4. Simulation results for normalised Gaussian, Lorentzian and Voigt lineshape profiles of the same area under the curve A = 1.

It is useful to estimate the order of magnitude of the broadening processes affecting measurements under typical experimental conditions. It helps with optimizing the experimental set-up when required, as well as helping to select the proper relation when performing some theoretical fit of acquired data. According to the previous discussion in this section, there are basically two experimental parameters that determine the final broadening contributions: the gas temperature and pressure. Typical conditions during the experimental work presented later are gas temperature of $T_{GAS} \approx 22$ °C and pressure $P_{GAS} \approx 1$ mbar. For these values the approximate order of magnitude for the natural, collisional, transit time and Doppler broadenings is respectively 100 Hz, 10 MHz, 50MHz and 500 MHz. The laser linewitdh was typically $\Delta\upsilon_{LAS} \approx$ 1-5 MHz. As it can be observed the broadening is

dominated by the Doppler effect at low pressure values. As pressure increases so does the collisional term, eventually dominating the total absorption linewidth at pressures above tens of millibars. The natural linewidth is negligible in this scenario. Note how the estimated values for these broadening processes –except the negligible natural linewidth term- are significantly higher than the typical emission frequency linewidth of the diode lasers utilised during experimental work.

3. Laser diodes in spectroscopy

3.1 Important parameters in laser spectroscopy

The absorption signals of gas species are not ideal in most real scenarios and acquiring good quality data is not a straightforward task. Low gas pressure or concentrations, rapidly changing temperature gradients within the targeted volume (ex. combustion jets in airplanes) or presence of multiple gases and overlap of gas absorption lines are examples of issues encountered in many real field experiments. For laser spectroscopy applications to be feasible, some parameters of the laser source become crucial and must be met:

- *Spectral purity (laser linewidth)*: the output from a laser source is broadened by several mechanisms, such as random phase changes due to spontaneous emission within the laser cavity or electronic noise from the laser current or temperature controllers. In most cases, a rule-of-thumb for successful gas absorption spectroscopy is that the laser linewidth should be smaller than 5% of the gas absorption linewidth.
- *Tuneability*: the output of the laser source must be ideally tuneable by using temperature or current control. A typical tuning range of 5 nm is required in multigas sensing applications (with typical temperature/current tuning rates of 0.1 nm/°C and 0.01 nm/mA respectively).
- *Modulation*: in order to apply high-sensitivity detection techniques such as WMS and FMS (see section 4.2), a high bandwidth modulation of the laser source is both desirable and necessary.

Additional parameters such as reduced size for portability, fiberized laser output for easier system integration, or cost-effective fabrication processes, are also beneficial for the design and implementation of effective gas detection schemes.

3.2 Widely tunable telecommunication laser diodes

Laser diodes (LD's) developed by the optical communications industry in the last decades are ideal candidates for spectroscopy studies, especially in the Infrared region where the absorption strength of some gases is significantly weak. An optical telecommunication window was opened in 1977 centred at 1550 nm (the *C-band*), so much effort was made to improve the performance of laser sources working in this Near Infrared (NIR) region of interest. These affordable LD's fulfil the linewidth characteristics required for spectroscopic applications, their emission frequency can be tuned across a wide range of values and they exhibit a great flexibility when modulation techniques need to be applied. Many different types of tuneable LD's (TLD's) exist that fulfil usual spectroscopic

requirements, based on different laser structures and tuning mechanisms. Some characteristics of two of these laser diodes, namely *SG-DBR (Sampled Grating Distributed Bragg Reflector)* and *SGC-DFB (Strongly Gain Coupled Distributed Feed Back)*, are summarized in table 1 as an example.

	SG-DBR (Sampled Grating Distributed Bragg Reflector)	SGC-DFB (Strongly Gain Coupled Distributed Feed Back)
WAVELENGTH RANGE (NM)	1535-1570	1537.5-1539.5
TUNING MECHANISM	Current	Current/Temperature

Table 1. Wavelength and tuning characteristics of two sample NIR tuneable laser diodes

A very detailed treatment on tuneable laser sources by Buus (Buus et al, 2005) can be consulted for further design and working principles applying to these types ofLD's.

4. Typical detection techniques

4.1 Direct absorption

The most simple and straightforward detection technique is that where the light is collected *directly* after it interacts with the absorbing gas or medium. The unmodulated emission wavelength of the laser is scanned across the spectral region of interest and the transmitted signal recorded using a photodiode/photodetector. A typical gas absorption line using this scheme is depicted in figure 5. As it can be observed, the absorption peak sits on the top of a sloped background. This slope is a result of the optical power of the laser being proportional to the scanning laser current/temperature. This is an undesired effect as it reduces the Signal-to-Noise Ration (SNR) of the collected data, and thus limits the maximum sensitivity achievable with this detection technique.

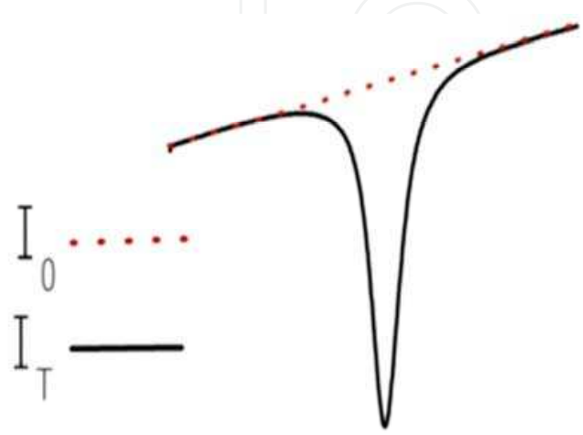

Fig. 5. Gas absorption signal utilizing a direct absorption technique.

4.2 Modulation techniques

In order to enhance the detection of weak absorption signals some high sensitivity techniques can be applied, based in the modulation of the emission wavelength of the laser diodes utilised. Two main techniques are commonly used, namely Wavelength Modulation Spectroscopy (WMS) and Frequency Modulation Spectroscopy (FMS).

In the case of WMS, the emission wavelength of the laser source is modulated at frequencies smaller than the FWHM of the absorption profile (≈ kHz/MHz). Modulation is typically achieved using an external sinusoidal signal applied to the modulation facility of the current controller driving the laser. Following the treatment by Reid and Labrie (Reid & Labrie, 1981), the emission frequency therefore may be written as

$$\upsilon(t) = \bar{\upsilon} + a\cos\phi_m t \tag{19}$$

Where $\bar{\upsilon}$ is the mean emission frequency, ϕ_m the angular modulation frequency and a the modulation amplitude. Because absorption is weak for the targeted gas transitions, the Beer-Lambert law presented in (8) can be approximated by the expression

$$I(\upsilon) = I_0(\upsilon)\left[1-\kappa(\upsilon)z_D\right] \quad = I_0(\upsilon)\left[1-\kappa(\bar{\upsilon}+a\cos\phi_m t)z_D\right] \tag{20}$$

The time dependent term, periodic and even function, can be expanded in a cosine Fourier series

$$\kappa(\bar{\upsilon}+a\cos\phi_m t) = \sum_{n=0}^{\infty} H_n(\bar{\upsilon})\cos(n\phi_m t) \tag{21}$$

Where $H_n(\bar{\upsilon})$ is the n^{th} Fourier component of the modulated absorption coefficient. The mean frequency is considered constant over a modulation period and the laser power assumed to remain constant while modulation occurs. Equation (21) essentially summarises the key aspect of this technique: demodulating the detected signal using a *Lock-In Amplifier* (LIA, (Bentham Electronics, 2009; John, 1994)) referenced at some multiple *nf* of the modulation frequency $f = \phi_m/2\pi$ makes the LIA output proportional to the n^{th} *Fourier component* according to $I_0(\upsilon)H_n(\bar{\upsilon})z_D$. A detailed theoretical analysis shows that such components are dependent on the absorption lineshape or its derivatives, so the above discussion means that, in practice, the output of a demodulator referenced at the n^{th} multiple of the laser modulation frequency is proportional to the n^{th} derivative of the absorption profile. A simple, more intuitive way of understanding this important result is presented by Suplee et al (Supplee, J. M. et al, 1994). If the small absorption coefficient $\kappa(\upsilon) << 1$ in (20) is expanded into a Taylor series around the mean frequency $\bar{\upsilon}$ one gets

$$I(\upsilon) = I_0(\upsilon)\left[1 - z_D\left(\kappa(\bar{\upsilon}) + \left.\frac{d\kappa}{d\upsilon}\right|_{\bar{\upsilon}}(\upsilon-\bar{\upsilon}) + \frac{1}{2!}\left.\frac{d^2\kappa}{d\upsilon^2}\right|_{\bar{\upsilon}}(\upsilon-\bar{\upsilon})^2 \ldots\right)\right] \tag{22}$$

which using (19) and applying trigonometric identities can be rewritten as

$$I(\upsilon) = I_0(\upsilon)\left[1 - z_D\left(\kappa(\bar{\upsilon}) + \left.\frac{d\kappa}{d\upsilon}\right|_{\bar{\upsilon}} a\cos(\phi_m t) + + \frac{1}{2!}\left.\frac{d^2\kappa}{d\upsilon^2}\right|_{\bar{\upsilon}} a^2 \frac{1}{2}\cos(2\phi_m t)...\right)\right] \quad (23)$$

Only terms up to second order have been considered, as higher terms for the Taylor expansion rapidly decay according to the weighting amplitude factor a^n (the modulation amplitude a in WMS experiments is usually small compared to the FWHM of the targeted absorption feature). Thus, equation (23) explicitly reveals the proportionality between the first and second derivatives of the absorption coefficient κ and the components of the transmitted intensity demodulated at frequencies ϕ_m and $2\phi_m$, respectively. Note that the unique Fourier transform of the absorption coefficient in (21) is essentially the same as the Taylor expansion, because trigonometric identities allows for terms in consecutive frequencies $n\phi_m$ to be grouped together. Figure 6 represents a typical schematic set-up when using this Lock-in detection technique.

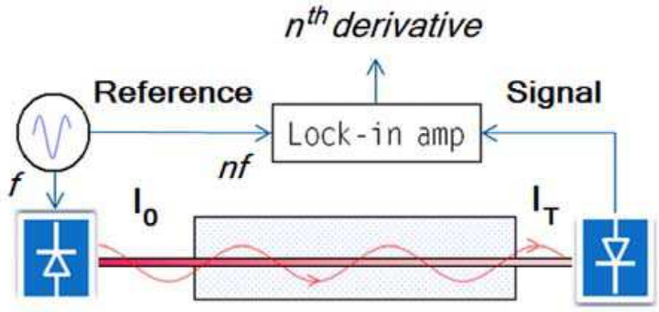

Fig. 6. Schematic diagram for a WMS lock-in detection technique.

It can be demonstrated that the amplitude of the detected n^{th} harmonic signal depends on the amplitude a of the modulation signal (*modulation depth)*, which in practice allows for optimization of the LIA output amplitude. A particular advantage of this WMS detection technique is that any residual sloped background detected in direct transmission measurements is effectively suppressed, significantly improving the Signal-to-Noise Ratio (SNR) of the acquired data.

The second case, FMS, is essentially based in the same principle as WMS, but only differs in the order of magnitude of the applied modulation frequency: In the FMS technique, the modulation frequency is much higher than the FWHM of the absorption line. The main effect of this high-frequency modulation is the appearance of several sidebands in the optical power spectrum of the laser source, separated from the carrier emission frequency υ_0 by an amount exactly equal to the modulation frequency f. The number of sidebands can be controlled by adjusting the modulation amplitude applied to the laser, with only the first sidebands typically considered. Several beat effects can occur between the sidebands and carrier peaks that may affect the detected signal, and must be assessed if some detailed information needs to be extracted. On the other hand, the main advantage of FMS detection is shifting the detection frequency to higher values where the low-frequency *1/f* noise affecting the laser is greatly reduced. However, the lock-in amplifier must be substituted by discrete high-frequency components which are more expensive and sensitive to external

noise coupling. Formal analysis of both WMS and FMS techniques can be found in references (Silver, 1992; Suplee et al, 1998).

4.3 Feedback techniques

It is common to find dynamic physical systems where one or more of the outputs drift with time and need to be stabilised to a reference value. These kind of systems are widely spread both at macroscopic and microscopic scales with examples including temperature regulation in buildings, microscopes where vibrations need to be minimised and effectively suppressed or cruise speed control associated with different means of transport such as cars or ships. In order to stabilise the desired output a certain signal is chosen which contains the relevant information to assess the stability, and then processed before being fed back to the system *S* implementing a loop structure. A schematic diagram corresponding to a simple case is presented in figure 7, where only one time-dependent output parameter needs to be stabilised and its magnitude *y(t)* become exactly equal to that of a chosen reference value *r(t)* at all times.

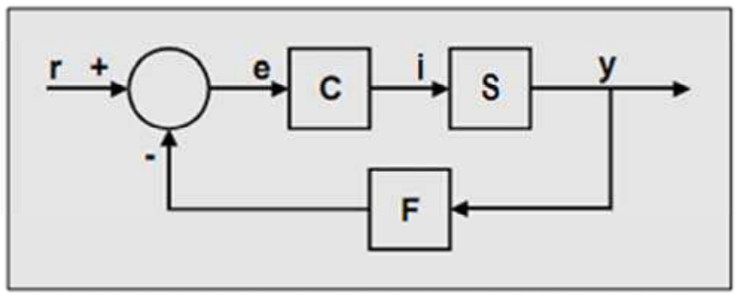

Fig. 7. Schematic diagram for a feedback control loop to stabilise a dynamic system S.

In the ideal case where the output is stable in time the condition $y(t) = r(t)$ holds. However, under normal operation conditions the magnitude of the output of interest drifts with time from the desired value. In that case the output signal is collected by a sensor scheme *F* and subtracted from the reference signal, defining a finite error signal $e(t) = r(t) - y(t)$. This signal is a measure of the departure of the system from its stable state and its magnitude relative to the output is typically small. A controller *C* receives this error signal and generates the input value *i(t)* to be finally fed back to the system *S*. In the ideal case of successful implementation of a stabilization loop this input value compensates the undesired system drift. The error value asymptotically approaches zero within some stabilizing time interval, which will be characteristic of the physical process involved in the system and can be defined as the system time constant τ_{SYS}. It is customary to define such an arrangement as an *active feedback loop*. Small signal analysis is usually applied in this type of loops as the magnitude of the error signal is much smaller than the system output, and compensation for the undesired drift thus carried out in a linear regime. Transient behaviour becomes important when the loop is initially closed, and conditions must be chosen to assure that the magnitude of the error signal does not exceed a certain limit during the associated transient time scale. On the other hand the frequency response of the loop is determined by its effective time response $\tau_{SYS,}$ and the active loop will be only able to compensate system drifts whose associated time scale τ_{DRIFT} is longer than that effective response.

Active feedback loops can be applied to stabilization of a laser output frequency. The emission frequency of a laser source exhibits some finite drift in time under normal operation conditions, mainly due to 1/f noise in the laser controllers. This becomes a serious drawback in fields where frequency stability plays a crucial role (such as optical metrology or precise frequency referencing), so active feedback loops can be applied to minimise such noise effects. Figure 8 includes the experimental scheme to implement an active feedback loop in order to lock the optical frequency $\upsilon(t)$ of a laser source, making use of a spectral feature of gas in an absorption cell. The laser optical frequency is now the output of the system to be stabilised $y(t) = \upsilon(t)$.

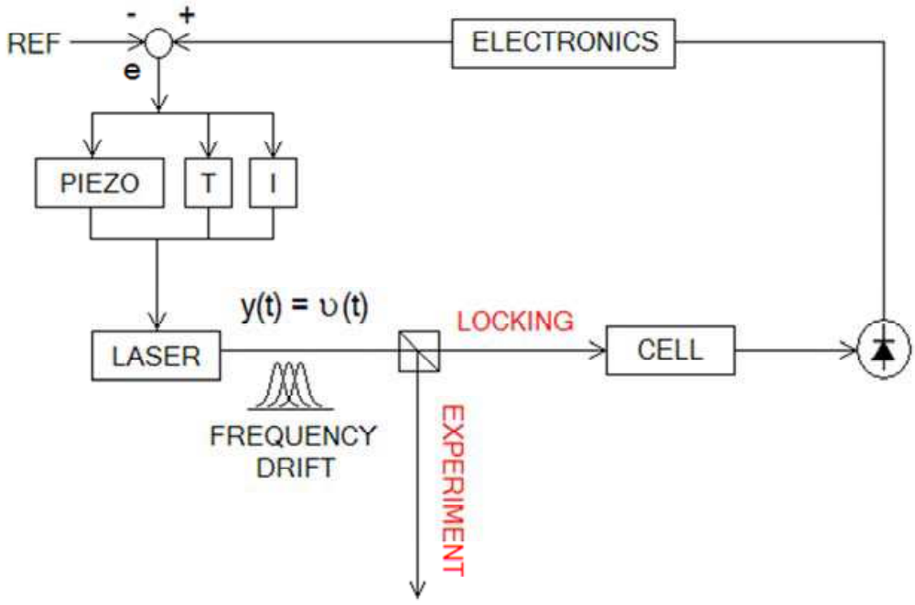

Fig. 8. Active feedback loop to lock the operating frequency of a laser, based in a gas absorption cell.

As observed in the figure, a usual arrangement is that where the main beam is divided in two with the help of a suitable splitting element. A small fraction is used for locking purposes, while the remaining light is sent towards the main experiment to be carried out.

5. An example: Gas sensing in hollow-core photonic bandgap fibres

Some experimental results are presented in this section to illustrate the various concepts covered so far, pointing out the main characteristics regarding the associated experimental scheme.

5.1 Hollow-core photonic bandgap fibres

Standard optical fibres work on the basis of the Total Internal Reflection (TIR) happening between the fibre core and cladding materials due to the step in the refractive index profile. However, a completely different guiding mechanism can be utilised based on the so-called *Photonic Crystal* (PC) structures (reference (Joannopoulos, 2008)). PC's are periodical

structures in which materials of different refractive index alternate according to the geometry imposed by a certain lattice configuration. By means of multiple interference effects, based on a detailed analysis of the Maxwell equations, either allowed or forbidden frequency states for photons arise within the PC structure. The total frequency interval across which light is not able to propagate defines the so-called *Photonic Band Gap* (PBF), analogous to semiconductors and *electronic* bandgaps. Thus, when a photonic bandgap structure is embedded within a standard silica fibre the new light guiding mechanism applies, giving rise to a *Photonic Bandgap Fibre* (PBF). In an ideal PBF the bandgap structure is designed so that only one fundamental mode is allowed to propagate along the fibre core length. Secondary modes rapidly decay across the surrounding fibre region due to the photonic band gap effect. A particular type of PBF is the so-called *Hollow-Core Photonic Bangap Fibre* (HC-PBF) (Benabid et al, 2005;Konorov et al, 2005; Ritari et al, 2005), characterized by a hollow core along with a surrounding array of air holes distributed according to a PC structure (figure 9). This type of fibre can easily be filled with either gaseous or liquid materials by standard pumping techniques or just by using capillary or diffusion effects.

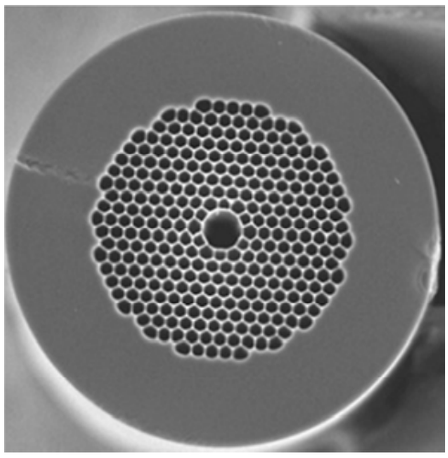

Fig. 9. Cross-section of a HC-PBF. Taken from (NKT Photonics, 2009).

5.2 Linear gas sensing in HC-PBF

Results are presented here regarding linear acetylene gas $^{12}C_2H_2$ hosted within a HC-PBF of core size ≈ 11 um. A SG-DBR laser diode operating at a wavelength $\lambda \approx 1530$ nm is coupled into the fibre using high precision translational stages and lenses. The fibre sits within a gas chamber at a gas pressure p = 5mbar and temperature T = 22 °C. The diffusion time of acetylene inside the hollow fibre structure is $t_{DIFF} \approx 10$ min. The emission wavelength of the LD is scanned using temperature and current controllers, and the transmitted signal of the gas collected using an InGaAs photodiode. High sensitivity WMS is achieved by means of current modulation of the LD, and the operating LIA referenced to the second harmonic (*2f*) of the modulation frequency. Results for several acetylene absorption lines are presented in figure 10, including signals from weakly absorbing lines that are enhanced due to the WMS technique. The particular shape of the 2f harmonics for selected gas lines around 1530 nm can be observed in the inset.

The results can be extended to the non-linear absorption regime by utilising a high-power laser diode. In such regime the absorbing transition gets saturated and the transmitted (absorbed) light is no longer directly proportional to the input optical power. The Beer-Lambert law given by equation 7 is no longer valid and a deeper theoretical analysis must be carried out in order to find out the analytical expression for the lineshape function $g(\nu-\nu_0)$ (a detailed analysis can be found in (Demtröder, 1996)). Non-linear absorption experiments are commonly based on the so-called *pump-probe* scheme, where an additional weak beam is used in conjunction with the high-power source in order to detect the nonlinear signal. This experimental arrangement is of particular complexity but can lead to many useful applications, such as stabilisation of the laser diode emission wavelength (Pineda Vadillo et al, 2009) by implementing an active feedback loop, as explained in section 4.3. Nonlinear absorption signals normally possess a very narrow spectral intensity profile so it is necessary to utilise laser diodes with ultranarrow emission linewidths, in order to prevent laser-induced broadening of the gas absorption lines.

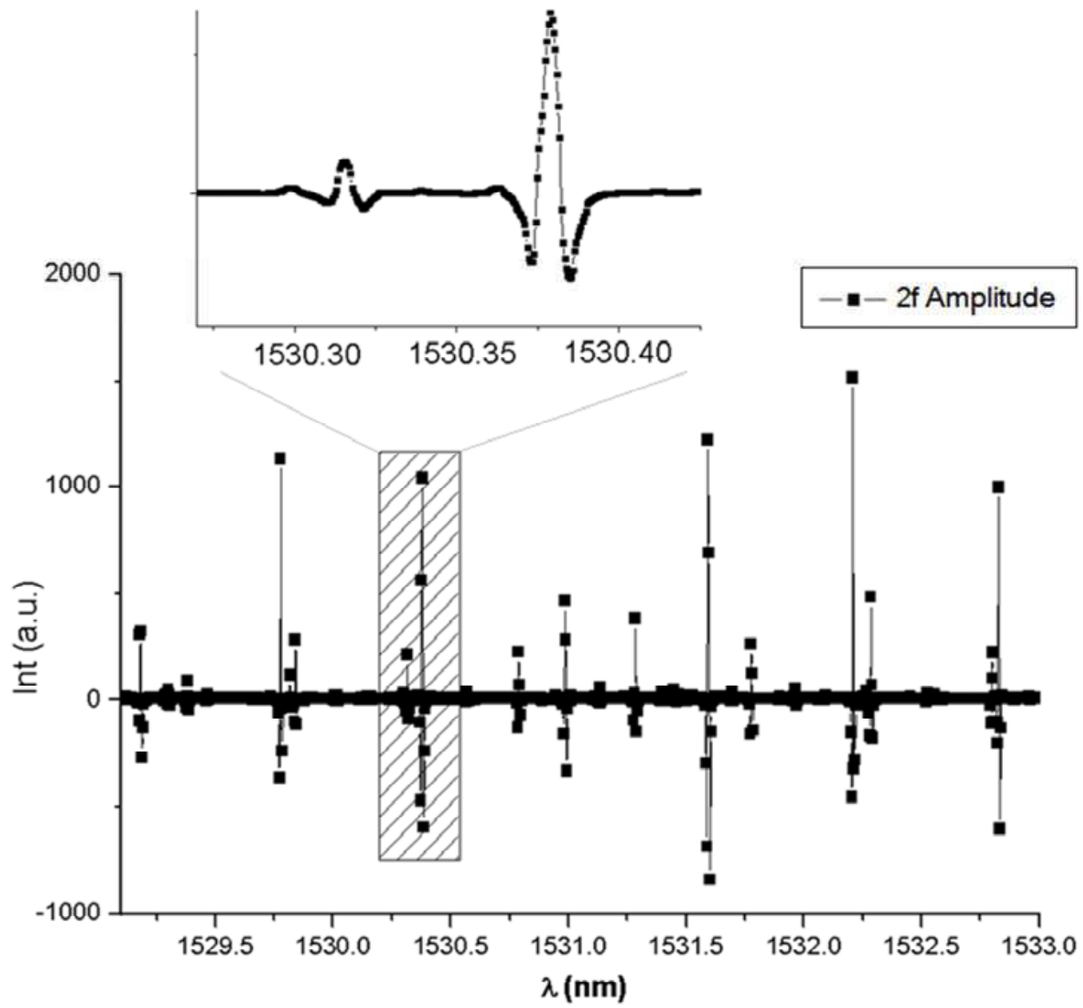

Fig. 10. Results for the successful WMS detection of the second harmonic of multiple acetylene absorption lines within a HC-PBF microstructured fibre.

6. Conclusion

Laser Diodes are a fundamental tool in spectroscopy research. Some of their fundamental physical properties, along with an affordable cost, make them nowadays an ideal light source for high precision and sensitivity spectroscopic measurement techniques. Their operational versatility makes them well-suited for both laboratory and field-based applications, ranging from metrology or laser stabilization techniques to monitoring of environmental important gases or safety gas detectors in industrial processes. In addition, laser diodes can be utilized in conjunction with novel types of photonic microstructures in order to further enhance their spectroscopic capabilities. Current research including ultra-narrow linewidth laser diodes (see for example the chapter by Dr. R. Phelan within this book) is even pushing the limits of spectroscopic applications further, making the near-future a promising time for this type of laser sources.

7. References

Banwell, C. N. & McCash, E. M. (1994). *Fundamentals of Molecular Spectroscopy,* McGraw-Hill.

Benabid, F. et al. (2005). Compact, stable and efficient all-fibre gas cells using hollow-core photonic crystal fibres, *Nature* 434, pp. 488-491.

Bentham Electronics. (2009). Lock-In Amplifier, www.bentham.co.uk/pdf/F225.pdf

Buus, J et al (2005). *Tunable Laser Diodes and Related Optical Sources,* Wiley-IEEE Press.

Demtröder, W. (1996). *Laser Spectroscopy: Basic Concepts and Instrumentation* (2nd Edition), Springer.

Garrett, P. P. (2006). Absorption and Transmission of light and the Beer-Lambert Law, www.physics.uoguelph.ca/~pgarrett/teaching/PHY-1070/lecture-21.pdf.

Herzberg, G. (1945). *Infrared and Raman Spectra of Polyatomic Molecules,* D. Van Nostrand Company, Inc.

Joannopoulos, J. D. (2008). *Photonic crystals : molding the flow of light,* Princeton University Press, Princeton.

John, H. S. (1994). Frequency-domain description of a lock-in amplifier, *American Journal of Physics* 62, pp. 129-133.

Konorov, S et al. (2005). Photonic-crystal fiber as a multifunctional optical sensor and sample collector, *Opt. Express* 13, pp. 3454-3459.

Lepère, M. (2004). Line profile study with tunable diode laser spectrometers, *Spectrochimica Acta Part A: Molecular and Biomolecular Spectroscopy* 60, pp. 3249-3258.

Measures, R. M. (1988). *Laser Remote Chemical Analysis,* John Wiley & Sons.

Nave, C. R. (2005). Kinetic Theory, Department of Physics and Astronomy, Georgia State University, hyperphysics.phy-astr.gsu.edu/hbase/Kinetic/kinthe.html, 2009.

NKT Photonics, "HC-1550-02 fibre datasheet, www.nktphotonics.com/side5334.html, 2009.

Pineda Vadillo, P. et al (2009). Non-resonant wavelength modulation saturation spectroscopy in acetylene-filled hollow-core photonic bandgap fibres applied to modulation-free laser diode stabilisation, *Opt. Express* 17, pp. 23309-23315.

Reid, J. & Labrie, D. (1981). Second-harmonic detection with tunable diode lasers — Comparison of experiment and theory, *Applied Physics B: Lasers and Optics* 26, pp. 203-210.

Ritari, H.et al (2005). Photonic Bandgap Fibers in Gas Detection, *Spectroscopy* 20, pp. 30-34.

Ritari, T. et al (2004). Gas sensing using air-guiding photonic bandgap fibers, *Opt. Express* 12, pp. 4080-4087.

Silver, J. A. (1992). Frequency-modulation spectroscopy for trace species detection: theory and comparison among experimental methods, *Appl. Opt.* 31, pp. 707-717.

Steinfeld, J. I. (2005). *Molecules and Radiation: An Introduction to Modern Molecular Spectroscopy* (Dover Reprint Edition).

Supplee, J. M. et al (1994). Theoretical description of frequency modulation and wavelength modulation spectroscopy, *Appl. Opt.* 33, pp. 6294-6302.

Svelto,O. (1998) *Principles of Lasers* (4th Edition), Springer.

Varghese, P.L. & Hanson, R. K. (1984). Collisional narrowing effects on spectral line shapes measured at high resolution, *Appl. Opt.* 23, pp. 2376-2385.

Weldon, V. (2005). Spectroscopic Based Gas Sensing Using Tuneable Diode Lasers, *Encyclopedia of Sensors*, C. A. Grimes, E. C. Dickey, and M. V. Pishko, eds., American Scientific Publishers.

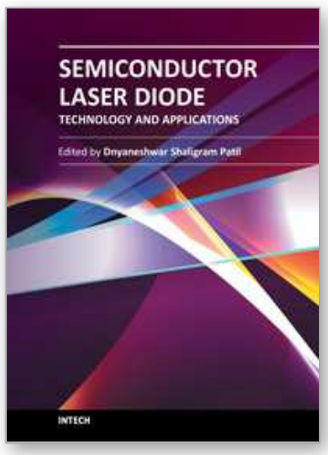

Semiconductor Laser Diode Technology and Applications
Edited by Dr. Dnyaneshwar Shaligram Patil

ISBN 978-953-51-0549-7
Hard cover, 376 pages
Publisher InTech
Published online 25, April, 2012
Published in print edition April, 2012

This book represents a unique collection of the latest developments in the rapidly developing world of semiconductor laser diode technology and applications. An international group of distinguished contributors have covered particular aspects and the book includes optimization of semiconductor laser diode parameters for fascinating applications. This collection of chapters will be of considerable interest to engineers, scientists, technologists and physicists working in research and development in the field of semiconductor laser diode, as well as to young researchers who are at the beginning of their career.

InTech Europe
University Campus STeP Ri
Slavka Krautzeka 83/A
51000 Rijeka, Croatia
Phone: +385 (51) 770 447
Fax: +385 (51) 686 166
www.intechopen.com

InTech China
Unit 405, Office Block, Hotel Equatorial Shanghai
No.65, Yan An Road (West), Shanghai, 200040, China
中国上海市延安西路65号上海国际贵都大饭店办公楼405单元
Phone: +86-21-62489820
Fax: +86-21-62489821

IntechOpen